Title	Resonant scattering of green light enabled by Ag@TiO2 and its application in a green light projection screen
Author(s)	Ye, Yiyang; Chen, Tupei; Zhen, Juyuan; Xu, Chen; Zhang, Jun; Li, Huakai
Citation	Ye, Y., Chen, T., Zhen, J., Xu, C., Zhang, J., & Li, H. (2018). Resonant scattering of green light enabled by Ag@TiO2 and its application in a green light projection screen. Nanoscale, 10(5), 2438-2446. doi:10.1039/C7NR07383F
Date	2018
URL	http://hdl.handle.net/10220/49176
Rights	

Nanoscale

PAPER

Resonant scattering of green light enabled by $Ag@TiO_2$ and its application in green light Projection Screen

Received 00th January 20xx,
Accepted 00th January 20xx

DOI: 10.1039/x0xx00000x

www.rsc.org/

Yiyang Ye,[a,*] T. P. Chen,[a,*] Juyuan Zhen,[b] , Chen Xu,[a] Jun Zhang,[a] Huakai Li[a]

The ability to selectively scatter green light is essential for a RGB transparent projection display, and this can be achieved by a silver-core, titania-shell nanostructure ($Ag@TiO_2$), based on metallic nanoparticle's localized surface plasmon resonance. The ability of selectively scattering of green light is shown in theoretical design, where structure optimization is included, and is then experimentally verified by characterization of a transparent film produced by dispersing such nanoparticles in polymer matrix. A visual assessesment indicates that a high quality green color image can be clearly displayed on the transparent film. For completeness, a theoretical design for selective scattering of red light based on $Ag@TiO_2$ is also shown.

I. Introduction

A transparent display enables us to see both the image displayed on it and the view behind it. Therefore, transparent display finds applications in, for example, augmented reality, which appears to show a floating object in air, and shop windows that can show translucent images and movies, and head up display which shows navigation information in a car's window shield. The market of Head Up Display is worth 9.02 Billion USD by 2020.[1] The revenue of VR/AR is expected to hit 150 billion USD by 2020.[2] Several types of transparent displays have been studied, each has its own advantages and disadvantages. Microlens array (MLA) can be used to implement a transparent display screen, but its fabrication process is complicated.[3] In the case of projection-based fluorescent display, three thin layers separately containing fluorescent materials emitting red, green and blue light upon absorbing their corresponding excitation light are stacked.[4] The projection-based fluorescent display is good in terms of transparency as well as the displayed image contrast ratio, but it must employ a specially designed projector that generates excitation wavebands. Organic light emitting diode (OLED) based screen is made by combining OLED and transparent electrodes such as indium tin oxide (ITO) glass. Despite the cost of OLED based screen can be theoretically made cheap by screen printing[5], and its advantage in flexibility, it suffers from the limited lifetime of the organic materials[6], and susceptibility to water and oxygen damage.[7] The most recently studied transparent display is the localized surface plasmon resonance (LSPR) based screens, which is theoretically achieved by dispersing into a visibly transparent matrix three kinds of specially engineered nanoparticles whose scattering peaks are sharp and are separately located around 630 nm (red light), 530 nm (green light) and 450 nm (blue light).[8] The advantage of the LSPR based screens is that the process to fabricate a film is simple and cheap given the engineered nanoparticles are ready. One way to achieve three sharp scattering peaks is by silver ellipsoids upon proper designing of shape and size, and array aligning.[9] However, upon normal illumination to the projection screen, strong, isotropic and sharp selective scattering enhancement has been experimentally demonstrated only for blue light based on LSPR effect.[8,10] Thus, it is of interest to find nanoparticles that enhance green- and red-light scattering.

In this work, nanoparticle of core-shell structure with silver as core and TiO_2 as shell ($Ag@TiO_2$) is theoretically found to selectively scatter green light while transmit light of other colours upon proper selection of its core and shell dimensions. This is then experimentally verified by measuring transmittance, extinction, absorption, forward and backward scattering spectrums of a transparent film made by dispersing the $Ag@TiO_2$ nanoparticles in polymer matrix. And the film's ability of displaying green-colour image is visually shown. The design and simulation for red light scattering is also discussed for completeness.

II. Theoretical design

In this section, the target is to find a nanoparticle that strongly scatters green light (around 530 nm) and transmit light of

[a] School of Electrical and Electronic Engineering, Nanyang Technological University, 639798 Singapore.
[b] University of Saskatchewan
Email: yeyi0005@e.ntu.edu.sg (Yiyang Ye), echentp@ntu.edu.sg (T.P. Chen)
† Footnotes relating to the title and/or authors should appear here.
Electronic Supplementary Information (ESI) available: [details of any supplementary information available should be included here]. See DOI: 10.1039/x0xx00000x

other colours. In other words, the nanoparticle should have a sharp peak at around 530 nm in the scattering spectrum, with small absorption, and the width of the peak should be as narrow as possible.

Reasons to choose Ag and TiO_2 to form core-shell structure

To achieve this target, metal nanoparticle's LSPR effect would be a choice.[11-14] As a rough estimation, quasi-static approximation (also called dipole approximation) is assumed in the following analysis.[15] For small metallic nanoparticles, according to Kreibig, the expression for resonance peak's halfwidth Γ^* is derived and given below:[16]

$$\Gamma^* = \frac{2\varepsilon_2(\omega)}{\sqrt{\left(\frac{d\varepsilon_1(\omega)}{d\omega}\right)^2 + \left(\frac{d\varepsilon_2(\omega)}{d\omega}\right)^2}}(1+\beta) \quad (1)$$

where $\varepsilon_1(\omega)$ and $\varepsilon_2(\omega)$ are respectively the real and imaginary parts of the dielectric function of the metallic material, ω is the incident light's frequency, the derivatives $d\varepsilon_1(\omega)/d\omega$ and $d\varepsilon_2(\omega)/d\omega$ are taken at resonance frequency $\omega = \omega_{resonance}$, β is an expression dependent on $\omega_{resonance}, \varepsilon_2(\omega), d\varepsilon_1(\omega)/d\omega, d\varepsilon_2(\omega)/d\omega$ and usually small (less than 2×10^{-3} in the case of silver) . According to (1), to make the width of the resonance peak narrow, either $\varepsilon_2(\omega_{resonance})$ should be small or $d\varepsilon_1(\omega)/d\omega$ should be large. As alkali metals are very unstable, only noble metals such as Au, Ag, Cu and Al can be considered. Actually Ag is the best candidate, because near the resonance peak wavelength of 530 nm, $\varepsilon_2(\omega)$ of Ag is less than 1, while $\varepsilon_2(\omega)$ of Au, Cu and Al are larger than 2 (Fig. 1).[17]

The condition for resonance under quasi-static approximation is [11, 12]

$$\varepsilon_1(\omega) = -2\varepsilon_m, \quad (2)$$

provided that $\varepsilon_2(\omega)$ is small or does not change much near the resonance, where ε_m is the surrounding medium's dielectric function.

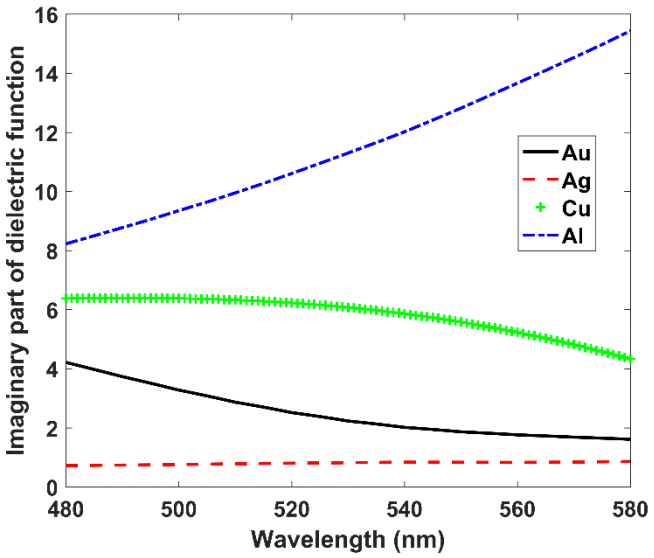

Fig. 1 Imaginary part of dielectric functions ($\varepsilon_2(\omega)$) around the 530 nm for Au, Ag, Cu and Al. Optical constants are taken from reference.[16]

However, the silver's resonance wavelength is around 400 nm according to equation (2), assuming the surrounding medium's refractive index is 1.5 (for most of polymer material). Thus, the next step is to shift the peak wavelength to 530 nm. It was suggested that both increasing a metallic nanoparticle's size and coating it with a high-refractive-index dielectric shell will redshift the resonance peak.[11]

By increasing the size alone has the following problem: although dipole-mode resonance peak will redshift, it decreases in strength, and the quadrupole mode will occur and gradually becomes dominant, resulting in an overall broad extinction spectrum.[11] As shown in (3), mathematically, the resonance condition for a metallic-core dielectric-shell structure, derived under quasi-static approximation,[18] explains why coating a metallic nanoparticle with a layer of high-refractive-index dielectric shell redshifts the resonance peak:

$$\varepsilon_1(\omega) = -2\varepsilon_{sh}\frac{(\varepsilon_{sh}+2\varepsilon_m) - \left(\frac{R}{R+d}\right)^3(\varepsilon_{sh}-\varepsilon_m)}{(\varepsilon_{sh}+2\varepsilon_m) + 2\left(\frac{R}{R+d}\right)^3(\varepsilon_{sh}-\varepsilon_m)} \quad (3)$$

provided that $\varepsilon_2(\omega)$ is small near the resonance wavelength, where ε_{sh} is the dielectric function of the shell (assumed to be constant), R and d are the core radius and shell thickness respectively. From equation (3), it is observed that increasing ε_{sh} requires $\varepsilon_1(\omega)$ to be more negative to meet the resonance condition. Since silver's $\varepsilon_1(\omega)$ decreases with increasing wavelength in the visible spectrum (400 nm ~ 800 nm),[17] the resonance peak redshifts when coated with a high-refractive-index dielectric shell. Intuitively, the redshift can be perceived in this way:[11] the dielectric shell reduces the surface charge, due to partial compensation by the polarization of the shell. The reduced surface charge corresponds to a smaller restoring force which in turn shifts the resonance frequency to lower values. In this work, TiO_2 is selected as the high-refractive-index dielectric shell. Thus, a possible nanoparticle that

selectively scatters green light is a core-shell structure with Ag as the core and TiO_2 as the shell ($Ag@TiO_2$).

Optimization consideration

The nanoparticles used in the experiments were synthesized in a specialized company (nanoComposix) based on our design and simulation results.

The diameter for the Ag core, and the thickness for the TiO_2 shell should be determined. For this purpose, the figure of merit (FOM) defined in reference is followed,[8] as given below:

$$FOM = \frac{\sigma_{sca}(\lambda_{resonance})}{2\overline{\sigma_{sca}} + \max\{\sigma_{abs}\}} \quad (4)$$

where the overline and the symbol $\max\{\dots\}$ respectively denote the mean and the maximum in the visible spectrum (from 400 nm to 800 nm), $\lambda_{resonance}$ is the resonance wavelength, σ_{sca} and σ_{abs} are the scattering and absorption cross sections respectively which can be calculated by the Mie's theory extended for core-shell structure.[19] The weighing factor (here it is 2) balances the sharp scattering and low absorption. This FOM favours the following properties: low absorption cross section over the whole visible spectrum, a high scattering cross section at the resonance wavelength, and low scattering cross section elsewhere, i.e. a narrow resonance peak.

With this FOM, the optimization for $Ag@TiO_2$ is carried out with the surrounding medium's refractive index assumed to be $n = 1.5$ (here PVA, polyvinyl alcohol is used). And TiO_2's refractive index is assumed to be 1.8. The choice of the value of TiO_2's refractive index is tentative. The reason why a low refractive index for TiO_2 is chosen rather than a value of 2.7[20] is that the chemical method employed produces amorphous TiO_2 shell,[21] which usually has a much lower refractive index than that of rutile phase due to lower density.[22] Later, it is shown that the actual refractive index of TiO_2 shell is even lower, down to 1.77, in order to make the calculated spectrum fit the measured extinction spectrum. The choice of the Ag's n, k values has to take into account the effect of surface scattering of electrons, since the silver core's size is comparable to electron's mean free path in bulk silver, which is about 52 nm.[23] The surface scattering of electrons will lead to an increased damping of free electrons. Thus, assuming silver nanoparticle's dielectric function is represented by a Drude-Lorentz model,[24] the extra damping γ_s caused by surface scattering of electrons is added to the bulk damping γ_b in the Drude term to give the corrected dielectric function ε_C for silver nanoparticle:[25]

$$\varepsilon_C = \varepsilon_{exp} + \frac{\omega_p^2}{\omega(\omega + i\gamma_b)} - \frac{\omega_p^2}{\omega[\omega + i(\gamma_b + \gamma_s]} \quad (5)$$

where ε_{exp} is silver's dielectric function from reference,[17] ω_p is the plasma frequency of silver, ω is the frequency of the incident light, i is the imaginary number. In the optimization, ω_p and γ_b are assumed to be 9.6 eV and 22.8 meV respectively.[25] And γ_s is given by:[26]

$$\gamma_s = \frac{Av_F}{r} \quad (6)$$

where $v_F = 1.39 \times 10^6 m/s$ is the electron velocity at the Fermi surface for silver,[25] and r is the radius of the silver core, A is a dimensionless fitting number, whose value is not free from controversy: values from 0.1 to 2 have been theoretically justified.[27] Since A values of 0.25, 0.8 have been experimentally reported,[26, 27] an A value of 0.5 is chosen for the optimization.

Table 1 Optimization results. The optimization starts with an initial guess of the shell thickness at each quantized diameter value.

Diameter (nm)	Initial guess of shell thickness (nm)	Locally optimized shell thickness (nm)	Optimized peak wavelength (nm)	Optimized FOM
40	45	115	527	0.5093
50	35	53	523	0.6541
60	25	42	538	0.8233
70	15	14	525	0.8941
75	10	7	520	0.9087
80	10	4	521	0.8543
100	5	0	540	0.6527

As the silver nanoparticles are readily available from the specialized company with the diameters of 5, 10, 20, 25, 30, 40, 50, 60, 70, 75, 80, 100, 110 nm, the $Ag@TiO_2$ nanoparticle's core diameters are quantized at these values.

Since the wavelength of green light is around 530 nm, the peak wavelength $\lambda_{resonance}$ should be tunable from 520 nm to 540 nm. The BOBYQA, a local optimization algorithm, is employed in the optimization process.[28] During the optimization, all diameter values are attempted. At each diameter value, an initial guess for shell thickness is given, and the FOM defined by equation (4) is maximized with two tunable variables: the shell thickness and the wavelength (bounded from 520 nm to 540 nm). The result for the optimization is given in Table 1. Although a 75 nm silver core with 7 nm shell has the highest FOM,

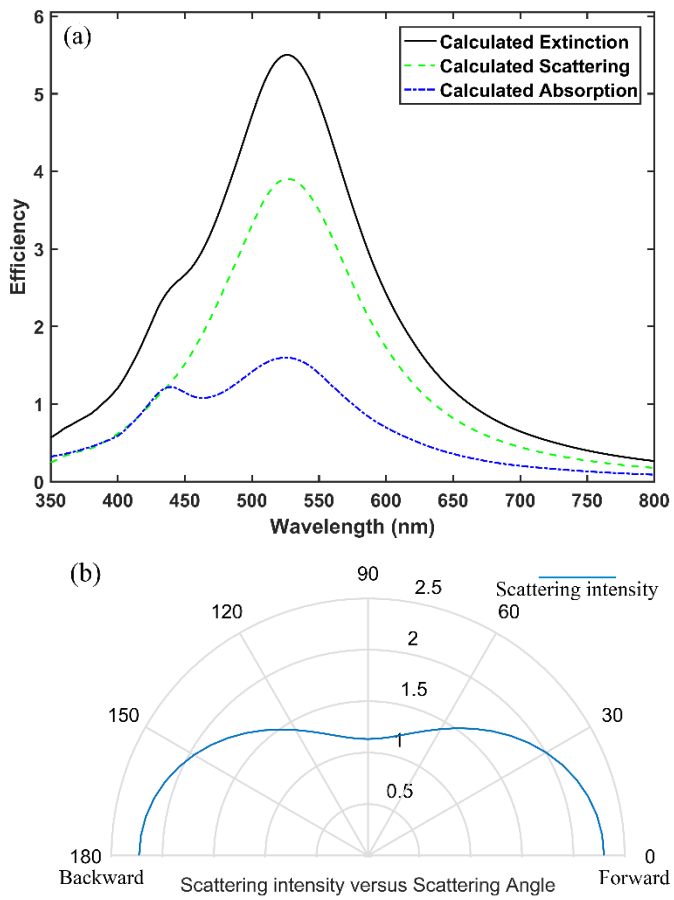

Fig. 2 (a) Efficiency (defined by $(cross\ section)/\pi a^2$, where $a = 49$ nm) for extinction, scattering and absorption, calculated by Mie's theory for the chosen target structure (core = 70 nm, shell thickness = 14 nm) as a function of wavelength. (b) Blue line represents intensity of the scattered light at resonant wavelength (525 nm) plotted versus the scattering angle (degree) in polar form, assuming incident light has a unit intensity, and equal components for the p- and s- polarization with respect to the scattering plane. Calculations are done by Mie's theory.

a TiO_2 shell with 7 nm thickness is difficult to synthesize. So, the structure with the second highest FOM (core = 70 nm, shell = 14 nm) is chosen as the reference target for synthesizing. And in Fig. 2, for this chosen reference target, the efficiency spectrums for extinction, scattering and absorption, and a polar diagram of the intensity of the scattered light at resonant wavelength (525 nm) calculated by Mie's theory are shown.

III. Experimental verification

The optimized structure (core = 70 nm, shell thickness = 14 nm) serves as a reference target for the experimental synthesis. Due to the difficulty in precisely controlling the size of the core (the core diameter shrinks during synthesizing) and shell, and the uncertainty in refractive index of amorphous TiO_2 shell caused by its low density,[22] the optimized size shown in Fig. 2 cannot be precisely synthesized and even so it may not give a satisfactory spectrum. In fact, of the many samples synthesized, it is found only the one with average core diameter of 67 nm and average shell thickness of 18 nm [Fig. 3] has a satisfactory spectrum characteristic with the peak

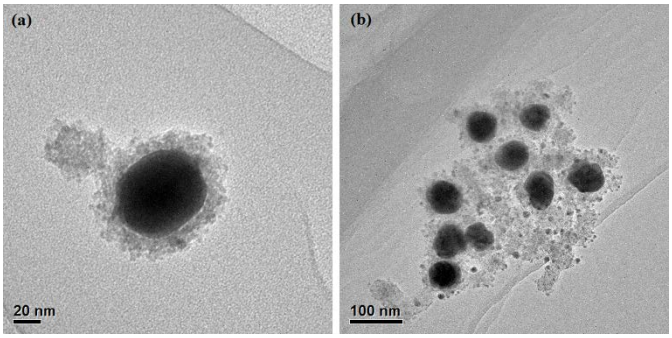

wavelength at 520 nm, a high scattering cross section around the peak wavelength and a low scattering cross section elsewhere, and an overall low absorption cross section.

The $Ag@TiO_2$ nanoparticles are originally dispersed in IPA (isopropanol) upon receiving, with a concentration of 0.49 mg/mL. To measure the haze, extinction and transmittance spectrums of the $Ag@TiO_2$ nanoparticles when their surrounding medium is polymer matrix, they are dispersed in PVA. And the procedures to make $Ag@TiO_2$-dispersed PVA film is as followings:

1. Add 3.57 g PVA (80% HYDROLYZED, SIGMA-ALDRICH) powder in 32 mL of deionized water (PVA has a weight percentage of 10%), and stir for 2~3 hours until PVA is fully resolved.
2. Degas the PVA water solution, if there is any bubble, in a vacuum chamber.
3. Add 2 mL $Ag@TiO_2$ IPA solution into the PVA water solution and stir for 10 minutes for the nanoparticle to be uniformly dispersed in the solution.
4. Pour the solution obtained into a square glass mould whose size is 10 cm by 10 cm, and put the mould in a fume hood for about 3 days.
5. After step 4, the dried PVA film dispersed with $Ag@TiO_2$ nanoparticle is ready, and is teared from the glass mold.

To measure the transmittance, extinction, absorption, scattering, ratio of forward and backward scattering of $Ag@TiO_2$ nanoparticles dispersed in PVA film, a pure PVA film is used for comparison, as described in section *Method*. For the fabrication of the pure PVA film, the procedures are the same as that for the $Ag@TiO_2$-dispersed PVA film with the exclusion of step 3.

Fig. 3 TEM images of the $Ag@TiO_2$ nanoparticles with average core diameter of 67 nm, average shell thickness of 18 nm. Fig. 3 (a) shows a single particle of such a core-shell structure. In Fig. 3 (b), free TiO_2 are observed.

Section *Method* describes how to derive the transmittance, extinction, absorption, scattering, forward and backward scattering spectrums of the $Ag@TiO_2$-dispersed PVA film from the optical measurements.

The transmittance spectrum of the $Ag@TiO_2$ nanoparticles dispersed in PVA film is measured (normalized against that of the pure PVA film) (Fig. 4) to show that light with wavelengths

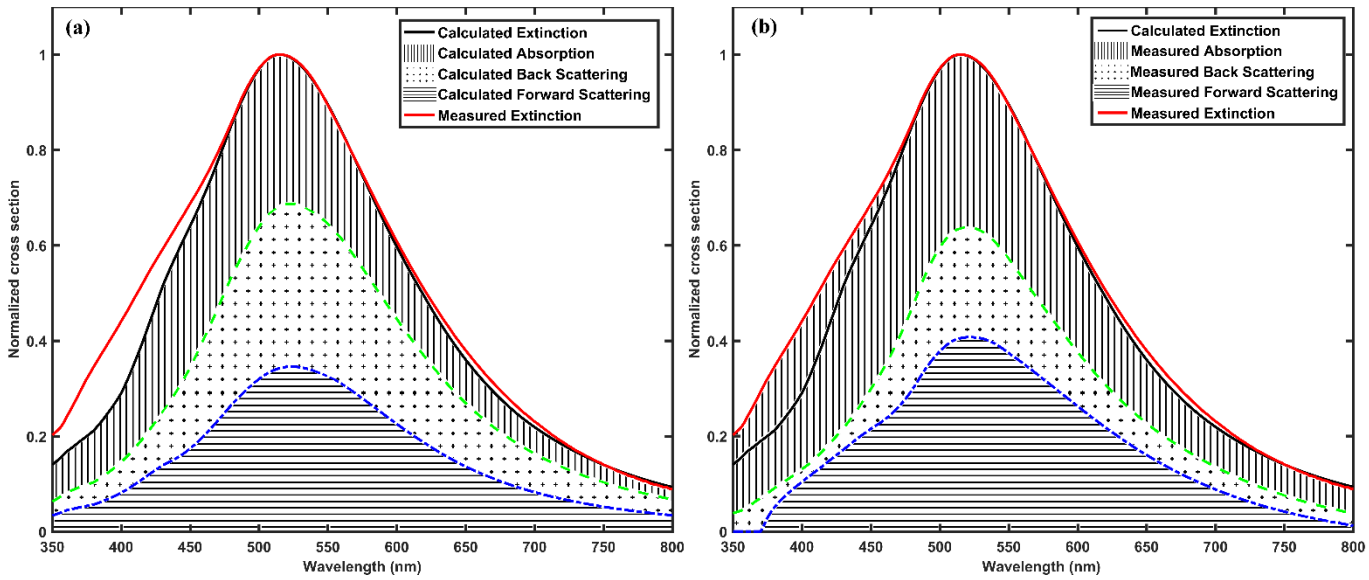

in the ranges away from 520 nm has a higher transmittance than that of light with wavelength near 520 nm. In Fig. 5, the measured extinction, absorption, scattering, forward and backward scattering spectrums are compared to those calculated by Mie's theory. In the calculations, the Ag's n, k values were surface-scattering corrected as described by equations (5) and (6), assuming the same parameters as in "Optimization consideration" part except that the A value is changed to 0.6, TiO_2 and surrounding medium's refractive indices were assumed to be 1.77 and 1.5, respectively, and a normal distribution of the nanoparticles with the core diameter of 67 nm with the standard deviation of 17 nm and the shell thickness of 18 nm with the standard deviation of 5 nm were assumed. The method to coat TiO_2 shell follows that described in reference.[21] The larger measured absorption in Fig. 5(b), as

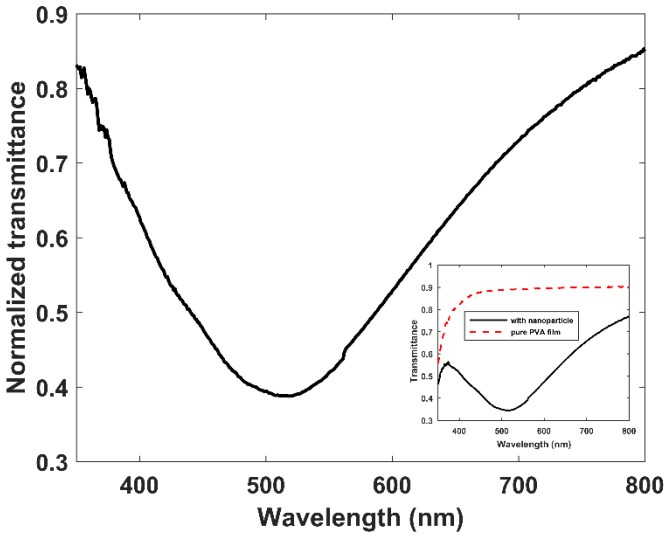

Fig. 4 Transmittance of the $Ag@TiO_2$-dispersed PVA film normalized to the pure PVA film, having an average value of 60.38%. The inset shows the comparison of the transmittance between the $Ag@TiO_2$-dispersed PVA film and the pure PVA film.

Fig. 5 Comparison between measured (red) and calculated (black) extinction spectrums, and components for absorption, forward and backward scattering calculated by Mie's theory in (a), and those derived from experimental measurements in (b). Note that the sum of the areas of forward and backward scattering gives the total scattering. The way to calculate forward and backward scattering with Mie's theory is to integrate the scattering light power from 0° to 90° and from 90° to 180° with respect to the scattering angle, respectively. The derivation of absorption, forward and backward scattering from experimental measurements is described in section "Method". The parameters used in the calculations are given in the text.

compared to that calculated in Fig.5 (a), may be due to absorption of PVA and free TiO_2 particles near the UV region, and measurement error or a larger damping of electrons' surface scattering (i.e. a larger value of A in equation 6) in the wavelength region from 420 to 800 nm. The measured back scattering is much smaller than the forward scattering around the resonant wavelength in Fig. 5(b) as compared to that in Fig. 5(a), this is due to the specular reflection exclusion port shown in setup $T_5(\lambda)$ Fig. 8 is very large, and some of the backscattered light is not captured by the integrating sphere. In the region away from the resonant wavelength, since the nanoparticles' scattering intensities are weak, the measurement of forward and backward scattering are susceptible to noise. A small gap is still observed between measured and calculated extinction in Fig. 5, which could be due to existence of free TiO_2 particles, and particle aggregation.

The effect of the green-light scattering of the $Ag@TiO_2$-dispersed film is clearly demonstrated by the high quality of the image of the green letters of "NTU" projected onto the film by a laser projector (SONY MP-CL1A), as shown in Fig. 6

(a). The green light generated from this projector is measured to be 523±3 nm. For comparison, the projected image onto the pure PVA film without the nanoparticle is also shown in the same figure. It can be observed from Fig. 6 (b) that the projected image of the three green letters on the pure PVA film is much poor. On the other hand, three RGB (red, green and blue) letters of "NTU" were placed behind the $Ag@TiO_2$-dispersed film. As shown in Fig. 6, the RGB letters can be clearly observed, showing a reasonably high transparency in the visible wavelength range. A supplementary video shows the isotropy of scattering.

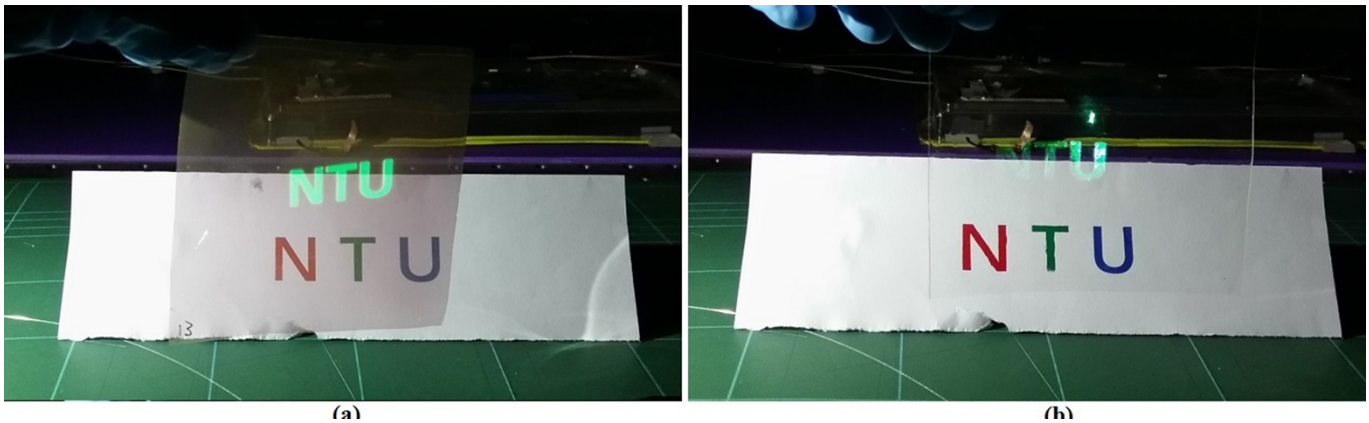

Fig. 6 Demonstration of the transparent nanoparticle-dispersed PVA film which selectively scatters green light (a). A pure PVA film without nanoparticle is shown for comparison (b). The images were projected by a laser projector (SONY MP-CL1A). The images of (a) and (b) are captured with the same lighting and exposure conditions, and the photographs are not edited.

IV. Theoretical design for red light scattering

It is worth mentioning that the $Ag@TiO_2$ structure may also be utilized for selective scattering of red light, upon proper selection of core and shell values. A similar optimization is carried out as described in section "II Theoretical design", all parameters are the same as in the optimization for green light scattering, except that a value of 2 is assumed here for refractive index of TiO_2, and the tunable range for peak wavelength $\lambda_{resonance}$ becomes 620 nm to 650 nm.

The optimized structure has a core diameter of 75 nm, shell thickness of 39 nm, a peak wavelength of 620 nm, with a FOM of 0.8921. The efficiency spectrums for extinction, scattering and absorption are plotted in Fig. 7 (a), and the polar diagram of the intensity of the scattered light at resonant wavelength (620 nm) is plotted in Fig. 7 (b).

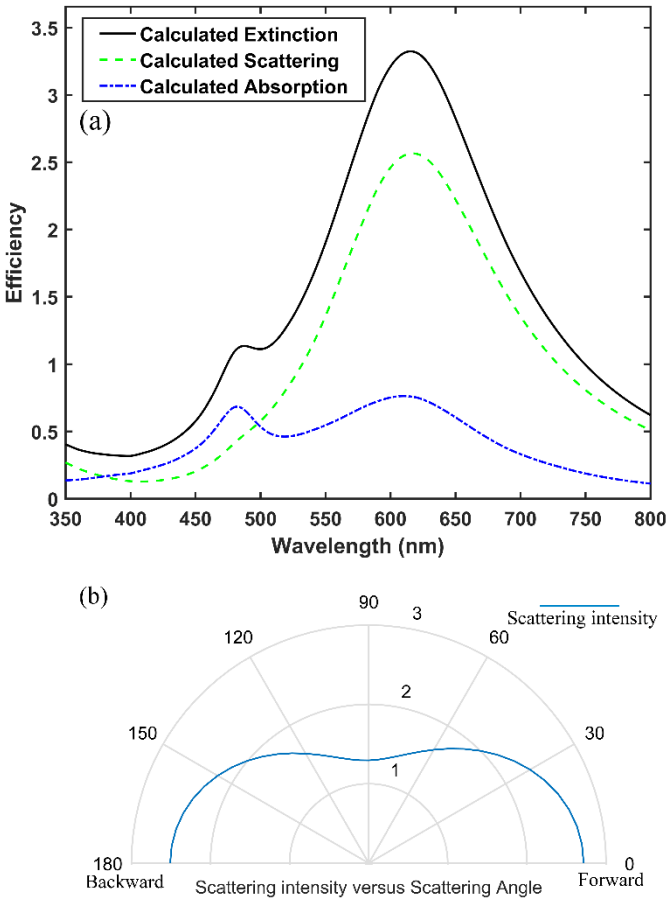

Fig. 7 (a) Efficiency (defined by $(cross\ section)/\pi a^2$, where $a = 76.5$ nm) for extinction, scattering and absorption, calculated by Mie's theory for the

structure with the highest FOM (core = 75 nm, shell thickness = 39 nm) as a function of wavelength. (b) Blue line represents intensity of the scattered light at resonant wavelength (620 nm) plotted versus the scattering angle (degree) in polar form, assuming incident light has a unit intensity, and equal components for the p- and s- polarization with respect to the scattering plane. Calculations are done by Mie's theory.

V. Method

The setup to measure transmittance, extinction, absorption, scattering, forward and backward scattering spectrums with an integrating sphere is improved from the one employed in the standard ASTM D 1003,[29] and is shown in Fig. 8, where T_i ($i = 1,2,3,4,5$) and R is proportional to the amount of light trapped in the integrating sphere, or in other words, the amount of light that fails to go out from the open port at the right side and, in the case of T_5's setup, the open port for the specularly reflected light to go out that is near the incident light port. And with the setup shown in Fig. 8, being similar to (but not the same as) the definition in ASTM D 1003, the haze value here of a film at a wavelength λ is defined as:

$$H(\lambda) = \frac{T_4(\lambda)}{T_2(\lambda)} - \frac{T_3(\lambda)}{T_1(\lambda)} \quad (7)$$

The haze value at a wavelength λ given by equation (7) shows the proportion of the forwardly scattered light among the total diffusely transmitted light, which consists of forwardly scattered light and directly transmitted light that goes in the same propagating direction of the incident light.

The derivation of nanoparticle's extinction spectrum employs the Beer-Lambert law. Considering the situation shown in Fig. 9, where $I_n(\lambda)$ ($n = 1,2,3,4$) denotes light intensity, and based on the Beer-Lambert law, the following equation can be obtained:

$$\frac{I_3(\lambda)}{I_2(\lambda)} = e^{-(N\cdot\sigma_{ext}+Noise)} \quad (8)$$

where N is the areal density of nanoparticles, i.e. number of nanoparticles per unit area (this area is perpendicular to the propagation direction of the incident light); σ_{ext} is the average extinction cross section of the nanoparticles dispersed in this film; and $Noise$ is due to scattering caused by the non-uniformity of the film itself.

Assuming that the loss of energy due to reflection and surface scattering at both the left air / film interface and the right film / air interface is x ($0 < x < 1$), we can write the following equations:

$$I_1(\lambda)(1-x) = I_2(\lambda) \quad (9)$$

$$I_3(\lambda)(1-x) = I_4(\lambda) \quad (10)$$

Equation (8) can thus be expressed as below in terms of $I_1(\lambda)$ and $I_4(\lambda)$:

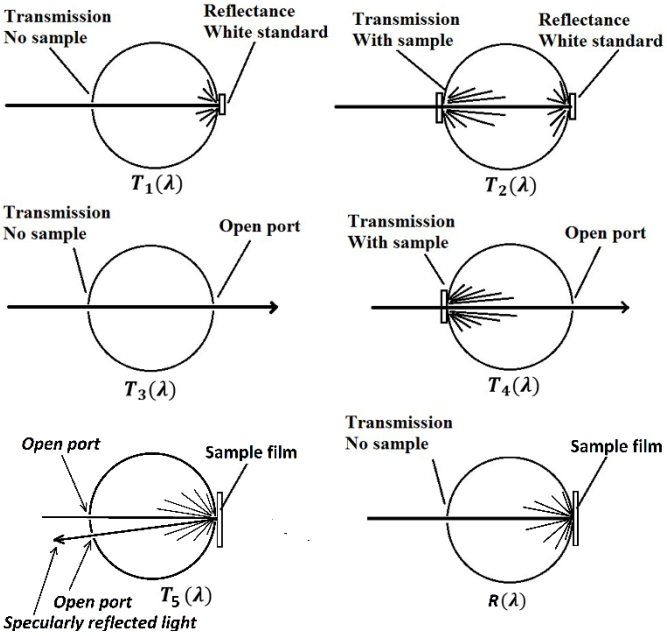

Fig. 8 Experimental setup to obtain a film's transmittance, extinction, absorption, scattering, ratio of forward and backward scattering values employing an integrating sphere. The directly measured values are $T_1(\lambda)$, $T_2(\lambda)$, $T_3(\lambda)$, $T_4(\lambda)$, $T_5(\lambda)$ and $R(\lambda)$ where T_i ($i = 1,2,3,4,5$) or $R(\lambda)$ is proportional to the amount of light trapped in the integrating sphere. The transmittance, extinction, absorption, scattering, ratio of forward and backward scattering values are deduced from these measured values.

$$\frac{I_4(\lambda)}{I_1(\lambda)(1-x)^2} = e^{-(N\cdot\sigma_{ext}+Noise)} \quad (11)$$

As both $I_4(\lambda)$ and $I_1(\lambda)$ are the light intensity in air, they are related to T_i ($i = 1,2,3,4,5$) by the same proportional constant α as below:

$$I_1(\lambda) = \alpha T_1(\lambda) \quad (12)$$

$$I_4(\lambda) = \alpha[1 - H(\lambda)]T_2(\lambda) \quad (13)$$

Therefore, equation (11) can be written as

$$\frac{[1-H(\lambda)]T_2(\lambda)}{T_1(\lambda)(1-x)^2} = e^{-(N\cdot\sigma_{ext}+Noise)} \quad (14)$$

Because the loss x and film-dependent $Noise$ are unknown, a pure film without any nanoparticle dispersed is used to eliminate the two parameters. A similar expression is derived with the same procedure under the assumption that the two parameters are about the same for the two films:

$$\frac{[1-H'(\lambda)]T_2'(\lambda)}{T_1(\lambda)(1-x)^2} = e^{-Noise} \quad (15)$$

where $H'(\lambda)\left(=\frac{T_4'(\lambda)}{T_2'(\lambda)} - \frac{T_3(\lambda)}{T_1(\lambda)}\right)$ is the haze value at the wavelength λ of the pure PVA film, $T_2'(\lambda)$ and $T_4'(\lambda)$ are measured for the pure film in the same way as for $T_2(\lambda)$ and $T_4(\lambda)$ for the nanoparticle-dispersed film. Note that $T_1(\lambda)$ and $T_3(\lambda)$ are not affected by the change of sample.

Now, $N \cdot \sigma_{ext}$ can be obtained from (14) and (15), as given below:

$$N \cdot \sigma_{ext} = -\ln\left(\frac{\left[1-\left(\frac{T_4(\lambda)}{T_2(\lambda)}-\frac{T_3(\lambda)}{T_1(\lambda)}\right)\right]T_2(\lambda)}{\left[1-\left(\frac{T_4'(\lambda)}{T_2'(\lambda)}-\frac{T_3(\lambda)}{T_1(\lambda)}\right)\right]T_2'(\lambda)}\right) \quad (16)$$

The $N \cdot \sigma_{ext}$, is the total extinction cross section within a unit

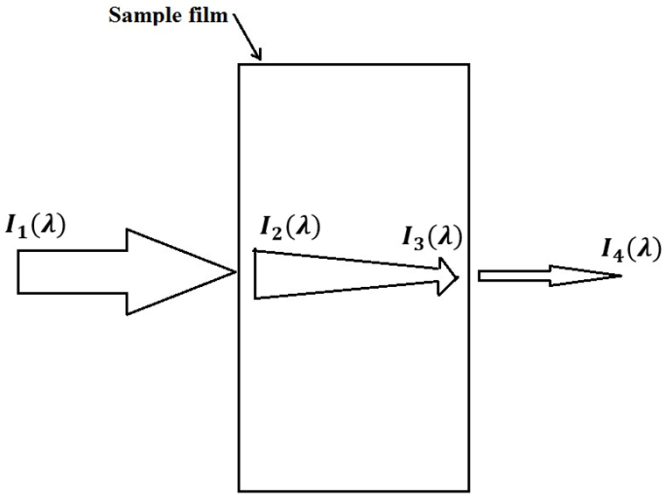

area, which was also named "extinction constant" in

Fig. 9 Schematic showing light attenuation when going through a thin film. $I_1(\lambda)$ denotes the incident light intensity. $I_2(\lambda)$ denotes the intensity for the light propagating in the original direction after a loss from $I_1(\lambda)$ at the left air / film boundary due to reflectance and surface scattering. $I_3(\lambda)$ denotes the intensity for the light propagating in the original direction after a loss from $I_2(\lambda)$ due to scattering and absorption during the course from the left air / film boundary to the right film / air boundary. $I_4(\lambda)$ denotes the intensity for the light propagating in the original direction after a loss from $I_3(\lambda)$ at the right film / air boundary due to reflectance and surface scattering.

reference.[11] Only $N \cdot \sigma_{ext}$ is derived from experimental measurements. This is because only the overall shape of the $N \cdot \sigma_{ext}$ spectrum that matters. The extinction spectrum $N \cdot \sigma_{ext}$ (red solid line) in Fig. 5 is normalized such that the maximum value of $N \cdot \sigma_{ext}$ is 1, and the rest values of this spectrum are scaled accordingly.

From Fig. 9 and equations (12) and (13), the transmittance shown in the inset of Fig. 4 is given by the following equation:

$$T(\lambda) = \frac{I_4(\lambda)}{I_1(\lambda)} = \frac{\left[1-\left(\frac{T_4(\lambda)}{T_2(\lambda)}-\frac{T_3(\lambda)}{T_1(\lambda)}\right)\right]T_2(\lambda)}{T_1(\lambda)} \quad (17)$$

To experimentally find the absorption and scattering components from the measured extinction spectrum, $N \cdot \sigma_{abs}$ is firstly derived from measurements in Fig. 8, where σ_{abs} is the average absorption cross section, in a way similar to that of deriving $N \cdot \sigma_{ext}$ employing Beer-Lambert law. Then, the scattering component is given by $(N \cdot \sigma_{ext} - N \cdot \sigma_{abs})$.

Assuming the PVA film is non-absorptive from 350 nm to 800 nm of light wavelength, then the intensity attenuation of the sum of diffusely transmitted light and diffusely reflected light compared to the incident light after it goes through the sample film is only due to absorption of the dispersed nanoparticles. Thus, with the measurement shown in Fig. 8, the following equation can be written:

$$\frac{\text{diffusely transmitted light} + \text{diffusely reflected light}}{incident\ light} = \frac{T_2(\lambda)+R(\lambda)}{T_1(\lambda)} = e^{-(N\cdot\sigma_{abs}+Noise)} \quad (18)$$

where $Noise$ comes from the PVA film and measurement system, and in the near UV region, $Noise$ includes PVA film's absorption. Assuming $Noise$ in the nanoparticle-dispersed film is the same as in the pure PVA film, the following equation can be written to eliminate the $Noise$ in equation (18).

$$\frac{T_2'(\lambda)+R'(\lambda)}{T_1(\lambda)} = e^{-Noise} \quad (19)$$

where $R'(\lambda)$ is the diffuse reflectance of the pure PVA film measured with the same setup as $R(\lambda)$. Thus, from equations (18) and (19), $N \cdot \sigma_{abs}$ is given by the following expression:

$$N \cdot \sigma_{abs} = -\ln\left(\frac{T_2(\lambda)+R(\lambda)}{T_2'(\lambda)+R'(\lambda)}\right) \quad (20)$$

Thus, the scattering component $N \cdot \sigma_{sca}$, where σ_{sca} is the average scattering cross section, is given by:

$$N \cdot \sigma_{sca} = N \cdot \sigma_{ext} - N \cdot \sigma_{abs} \quad (21)$$

Assuming the nanoparticles' forward scattering intensity $I_{Forward\ Sca}$ is proportional to the right-hand side of the following expression with proportional constant β:

$$I_{Forward\ Sca} \propto \frac{\left(H(\lambda)\cdot T_2(\lambda) - H'(\lambda)\cdot T_2'(\lambda)\right)}{T_1(\lambda)} = F \quad (22)$$

, and the nanoparticles' backward scattering intensity $I_{Back\ Sca}$ is proportional to the right-hand side of the following expression with the same proportional constant β:

$$I_{Back\ Sca} \propto \frac{\left(T_5(\lambda) - T_5'(\lambda)\right)}{T_1(\lambda)} = B \quad (23)$$

where $T_5'(\lambda)$ is the pure PVA film's back scattering measured with the same setup as for $T_5(\lambda)$. Then, the ratio of forward scattering $RA_{Forward\ Sca}$, and of backward scattering $RA_{Back\ Sca}$ are given by equations (24) and (25) respectively:

$$RA_{Forward\ Sca} = \frac{F}{F+B} \quad (24)$$

$$RA_{Back\ Sca} = \frac{B}{F+B} \quad (25)$$

VI. Conclusions and future work

In this work, a $Ag@TiO_2$ core-shell nanoparticle is proposed and demonstrated to achieve the objective of selectively scattering of green light. A transparent projection film is made

from this nanoparticle. Since the nanoparticles that enhances blue light scattering have been reported previously, with the demonstration of selectively scattering of green light in the present work people are one step closer to achieving a transparent LSPR-based RGB projection screen.

Since the scattering peak shown in this work is still not ideally narrow, future works include further reducing the size distribution of the nanoparticle, and maybe finding a blue-scattering particle having a resonant wavelength more blue-shifted as compared to that shown in ref,[8] and a red-scattering particle having a resonant wavelength around 725 nm, to leave enough wavelength space for transmitting lights with wavelength away from the three RGB resonance peaks.

Conflicts of interest

There are no conflicts to declare.

Acknowledgements

This work was financially supported by the National Research Foundation of Singapore (Program Grant No. NRF-CRP13-2014-02). Assistance provided by Dr Dingyuan Tang's group to measure laser projector's spectrum is also acknowledged.

Notes and references

1 Head-Up Display Market by Component (Video Generator, Projector, Software, Combiner and Others), Application (Military & Civil Aviation, and Automotive, Premium/Luxury Cars, Sports Cars, and Mid-Segment Cars), and Geography - Global Forecast to 2020, http://www.marketsandmarkets.com/Market-Reports/head-up-display-hud-market-684.html, (accessed 8th July, 2017).
2 Augmented/Virtual Reality Report Q3 2017 (major update for mobile AR), http://www.digi-capital.com/reports/#augmented-virtual-reality, (accessed 8th July, 2017).
3 M. K. Hedili, M. O. Freeman and H. Urey, *Appl. Opt.*, 2013, **52**, 1351-1357.
4 T. Sun, G. Pettitt, N. T. Ho, K. Eckles, B. Clifton and B. Cheng, 2012.
5 D. A. Pardo, G. E. Jabbour and N. Peyghambarian, *Adv. Mater.*, 2000, **12**, 1249-1252.
6 B. Geffroy, P. Le Roy and C. Prat, *Polym. Int.*, 2006, **55**, 572-582.
7 J.-S. Park, H. Chae, H. K. Chung and S. I. Lee, *Semicond. Sci. Technol.*, 2011, **26**, 034001.
8 C. W. Hsu, B. Zhen, W. Qiu, O. Shapira, B. G. DeLacy, J. D. Joannopoulos and M. Soljačić, *Nat. Commun.*, 2014, **5**, 3152.
9 A. Monti, A. Toscano and F. Bilotti, *Journal of Applied Physics*, 2017, **121**, 243106.
10 K. Saito and T. Tatsuma, *Nanoscale*, 2015, **7**, 20365-20368.
11 U. Kreibig and M. Vollmer, *Optical properties of metal clusters*, Springer Science & Business Media, 2013.
12 K. L. Kelly, E. Coronado, L. L. Zhao and G. C. Schatz, *J. Phys. Chem. B*, 2003, **107**, 668-677.
13 T. Hollstein, U. Kreibig and F. Leis, *physica status solidi (b)*, 1977, **82**, 545-556.
14 P. K. Jain, K. S. Lee, I. H. El-Sayed and M. A. El-Sayed, *J. Phys. Chem. B*, 2006, **110**, 7238-7248.
15 C. F. Bohren and D. R. Huffman, *Absorption and scattering of light by small particles*, John Wiley & Sons, 2008.
16 U. Kreibig, *Appl. Phys. A*, 1976, **10**, 255-264.
17 E. D. Palik, *Handbook of optical constants of solids*, Academic press, 1998.
18 M. Quinten, *Optical properties of nanoparticle systems: Mie and beyond*, John Wiley & Sons, 2010.
19 W. Yang, *Appl. Opt.*, 2003, **42**, 1710-1720.
20 J. R. DeVore, *J. Opt. Soc. Am.*, 1951, **41**, 416-419.
21 Z. W. Seh, S. Liu, M. Low, S.-Y. Zhang, Z. Liu, A. Mlayah and M.-Y. Han, *Adv. Mater.*, 2012, **24**, 2310-2314.
22 D. Mergel, D. Buschendorf, S. Eggert, R. Grammes and B. Samset, *Thin Solid Films*, 2000, **371**, 218-224.
23 U. Kreibig and C. v. Fragstein, *Zeitschrift für Physik*, 1969, **224**, 307-323.
24 P. Jahanshahi, M. Ghomeishi and F. R. M. Adikan, *The Scientific World Journal*, 2014, **2014**, 6.
25 M. G. Blaber, M. D. Arnold and M. J. Ford, *The Journal of Physical Chemistry C*, 2009, **113**, 3041-3045.
26 S. Berciaud, L. Cognet, P. Tamarat and B. Lounis, *Nano Letters*, 2005, **5**, 515-518.
27 B. S. Lucía and O. T. Jorge, *Nanotechnology*, 2006, **17**, 1309.
28 M. J. Powell, *Cambridge NA Report NA2009/06, University of Cambridge, Cambridge*, 2009.
29 H.-L. Yu and C.-C. Hsaio, *Metrologia*, 2009, **46**, S233.